Bone 120 (2019) 336–346

Contents lists available at ScienceDirect

Bone

journal homepage: www.elsevier.com/locate/bone

Full Length Article

A new noninvasive mechanical bending test accurately predicts ulna bending strength in cadaveric human arms

Lyn Bowman[a,b], Emily R. Ellerbrock[a], Gabrielle C. Hausfeld[c], Jennifer M. Neumeyer[a], Anne B. Loucks[a,b,*]

[a] Department of Biological Sciences, Ohio University, Athens, OH 45701, United States of America
[b] Ohio Musculoskeletal and Neurological Institute, Ohio University, Athens, OH 45701, United States of America
[c] Honors Tutorial College, Ohio University, Athens, OH 45701, United States of America

ARTICLE INFO

Keywords:
Cortical bone
Bone mechanics
Cortical porosity
Ulna
Bone strength
Bone fragility

ABSTRACT

Background: High error rates in the prediction of fragility fractures by bone mineral density have motivated searches for better clinical indicators of bone strength, and the high incidence of non-hip, non-spine fractures has raised interest in cortical bone. The aim of this study was to assess the accuracy of Cortical Bone Mechanics Technology™. CBMT is a new non-invasive 3-point bending technique for measuring the mechanical properties of cortical bone in the ulnas of living humans.

Methods: 35 cadaveric human arms were obtained from small women and large men ranging widely in age ($17 < Age < 99$ years) and body size ($14 < BMI < 40\ kg/m^2$). Noninvasive CBMT measurements of the flexural rigidity of the ulna bones within these arms (EI_{CBMT}) were compared to measurements of EI by Quasistatic Mechanical Testing in the ulnas excised from those arms (EI_{QMT}). Ulna bending strength was also measured by QMT as the peak moment before fracture (M_{peak}). The open source *BoneJ* plugin to *ImageJ* image processing software was used to calculate cortical porosity (CP) in micro-computed tomography images of a 2 mm length of the mid-shaft of each fractured ulna, and the interosseous diameter (IOD) of each ulna was also measured in those images.

Results: EI_{CBMT} measurements ($13 < EI_{CBMT} < 97\ Nm^2$) explained 99% of the variance in QMT measurements of ulna bending strength ($11 < M_{peak} < 90$ Nm), but EI_{CBMT} was biased high by 30% ($p < 0.0001$) relative to EI_{QMT} ($11 < EI_{QMT} < 69\ Nm^2$). After correcting this bias, EI_{CBMT} and EI_{QMT} measurements lay along the identity line ($y = 1.00x$, $R^2 = 0.99$, $SEE = 3.1\ Nm^2$). Predictions of M_{peak} by EI_{CBMT} were less accurate than predictions by EI_{QMT} (both $R^2 = 0.99$; $SEE_{CBMT} = 5.9$ Nm vs $SEE_{QMT} = 4.5$ Nm, $F = 2.92$, $p = 0.001$), but EI_{CBMT} predictions were substantially more accurate than those by IOD ($R^2 = 0.79$; $SEE_{IOD} = 10.6$ Nm, $F = 3.30$, $p < 0.001$) and CP ($R^2 = 0.35$; $SEE_{CP} = 18.9$ Nm, $F = 10.45$, $p < 10^{-9}$). Predictions by EI_{CBMT} were also more accurate than predictions by arm donor height ($R^2 = 0.63$; $SEE = 14.3$ Nm, $F = 5.87$, $p < 10^{-6}$), body weight ($R^2 = 0.77$; $SEE = 11.1$ Nm, $F = 3.54$, $p < 0.001$) and BMI ($R^2 = 0.64$; $SEE = 14.1$ Nm, $F = 2.39$, $p < 0.01$). In forward stepwise multiple regression beginning with EI_{CBMT}, only age explained any additional variance in ulna bending strength ($\Delta R^2 = 0.3\%$, $F = 8.03$, $p = 0.008$).

Conclusion: Noninvasive CBMT measurements of ulna EI explain 99% of individual differences in QMT measurements of ulna bending strength in cadaveric human arms.

1. Introduction

Fragility fractures cause pain, disability and more deaths among women than breast cancer, heart attack and stroke combined [1]. They occur frequently among the elderly, are complications of various diseases, and side-effects of several disease treatments. As a result, fragility fractures are a major burden on health care systems with annual costs approaching $25 billion in the United States [2] and $35 billion in Europe [3].

Abbreviations: CBMT, cortical bone mechanics technology; QMT, quasistatic mechanical testing; CP, cortical porosity; IOD, interosseous diameter; R^2, coefficient of determination; SEE, standard error of the estimate

* Corresponding author at: Department of Biological Sciences, Ohio University, Athens, OH 45701, United States of America.
E-mail address: loucks@ohio.edu (A.B. Loucks).

https://doi.org/10.1016/j.bone.2018.11.018
Received 23 July 2018; Received in revised form 5 November 2018; Accepted 25 November 2018
Available online 26 November 2018

1.1. The difficulty of targeting fracture preventive care

Effective treatments are available to prevent fragility fractures [4], but targeting this care at patients with weak bones is hampered by lack of a medical device that reliably identifies patients with weak bone. Since 1994, preventive care has been offered to patients whose areal bone mineral density (aBMD) measured by Dual-Energy X-ray Absorptiometry falls below the World Health Organization (WHO) diagnostic criterion for osteoporosis [5] — even though the inability of aBMD to distinguish between patients who had and had not fractured in the past was widely known even at that time [6]. Subsequent prospective studies have found that aBMD did not predict which patients would fracture in the future either [7–10]. The largest such study of 261,000 post-menopausal American women [7] found that 96% of those diagnosed with osteoporosis did not fracture during the follow-up observation period, while 81% of fractures occurred in women who were not osteoporotic. Another site-specific study found that only 10% (heel) to 44% (clavicle) of fractures could be attributed to osteoporosis [8].

To better identify patients who would benefit from fracture prevention care, in 2011 the FRAX® questionnaire was introduced. FRAX® estimates fracture risk by assessing clinical risk factors for fracture [11,12]. Since 2011, the FRAX® web page has logged 8000 such assessments per day. Unfortunately, prospective studies have found that FRAX does not predict fractures well either. Among post-menopausal French women, 74% of those identified by FRAX® as being at high risk for a major osteoporostic fracture did not fracture during follow-up, while 82% of fractures occurred in women identified as low risk [13]. Moreover, a meta-analysis of studies investigating the performance of FRAX using USA treatment guidelines found that FRAX failed to identify 90% of major osteoporotic fractures [14]. Thus, physicians still lack a reliable tool for targeting preventive care at patients with weak bone.

1.2. Measures of cortical bone

One reason aBMD fails to predict fractures well is that it explains only 50–80% of the variation in bone strength [15–20]. Moreover, the WHO diagnostic criterion for osteoporosis applies to spine and hip sites where most bone tissue is trabecular, whereas after age 60 most bone loss is cortical [21]. Among 51,000 women over 55 years of age in 10 countries, there were five times more non-hip, non-spine fractures requiring twice as many days of hospitalization, rehabilitation and nursing home care than hip and spine fractures combined [22]. Fifty percent of such non-hip, non-spine fractures occur in the arm [23]. Thus, a new tool for targeting preventive care at patients with weak cortical bone might be especially helpful for reducing the high costs of fracture treatment and misdirected preventive care.

In 2010, the observation that the increased incidence of fractures after age 60 is associated with an increased rate of cortical bone loss led to cortical porosity being proposed as an indicator of bone fragility [21]. Since then, cortical porosity has been the subject of extensive study [24]. Proponents of the method, in which cortical porosity is quantified in HRpQCT images of the distal radius and tibia, acknowledge two sources of error: inadequate spatial resolution in HRpQCT to accurately quantify cortical porosity, and ambiguity about the location of the boundary between true trabecular bone and “trabecularized” cortical bone at the imaging sites [25]. The rate of change in cortical porosity distinguishes perimenopausal and postmenopausal women [26], but in the previously cited study of post-menopausal French women, 77% of those with high cortical porosity (> 20%) did not fracture, while 67% of fractures occurred in women with low cortical porosity [13].

Bone strength cannot be measured directly in vivo, because one must break a bone to know how strong it used to be. However, bone strength has long been known to be strongly associated with non-destructive measurements of bone stiffness ($r > 0.95$) [27–30]. The gold standard reference method for measuring bone stiffness and strength is Quasistatic Mechanical Testing (QMT), but this technique cannot be used clinically because the first step in the method is to remove the bone from the body.

Reference Point Indentation (RPI) is an invasive hardness test of cortical bone. In RPI, an incision is made down to the bone, the periosteum of the bone is removed, a small stylus is driven a short distance into the cortical bone surface, and the resulting indentation depth is measured. The technique has been extensively studied [31], and it has been able to detect significant differences between cohorts in clinical research [32], but these measurements have been only weakly associated with any mechanical property of bone ($R^2 \leq 0.33$) [33–35]

Mechanical Response Tissue Analysis (MRTA) was a non-invasive method for measuring the mechanical properties of long bones in living humans. This dynamic 3-point bending test applied a spectrum of oscillatory forces to the skin overlying a long bone and analyzed the resulting frequency response of mechanical vibrations to make direct, functional measurements of the underlying bone's bending mass, stiffness and damping in situ [36]. Bending tests are especially useful for measuring the mechanical properties of cortical bone, because they are specifically sensitive to mechanical properties at the mid-span of a long bone, where bone tissue is entirely cortical.

The utility of MRTA was also extensively studied [37], but little was published about its measurement accuracy. The results of the only such animal study were unimpressive and acknowledged by the investigators to be confounded by differences between in vivo MRTA and ex situ QMT test conditions [29,38]. Moreover, a study of humans in vivo found excessive variability in repeated measurements in a single session with coefficients of variation up to 65% [39].

Because we were interested in reports of MRTA detecting changes in bending stiffness in the absence of changes in bone mineral [40–42], we investigated and identified sources of error in MRTA and developed techniques for overcoming them. We call these proprietary techniques Cortical Bone Mechanics Technology (CBMT). We focused attention on the ulna bone in the forearm, because of its superficiality under a thin layer of skin and its uniquely near-ideal biomechanics in bending. We then compared QMT and our new methods in 39 artificial human ulna bones [43]. These artificial bones had nominally identical geometry with controllably varied amounts of glass fill in the epoxy emulating cortical bone. Across the resulting range of stiffness, we found the relationship between CBMT and QMT measurements of bending stiffness to be indistinguishable from the identity line ($R^2 = 0.999$).

We have since tested 35 cadaveric arms donated by men and women varying widely in age and body size. Our CBMT measurements of the flexural rigidity of ulna bones in these arms are reported here, along with estimations of their bending strength, relative to measurements of the flexural rigidity and strength of the same ulnas by QMT. We also compared CBMT predictions of ulna bending strength to predictions by cortical porosity and various measures of ulna and whole body size.

2. Materials and methods

2.1. Specimens

To obtain a wide range of ulna stiffness and strength, we obtained 35 fresh-frozen cadaveric human arms from small women (BMI < 20 kg/m^2) and large men (BMI > 25 kg/m^2) in three age groups (< 65, 65–80 and > 80 years) from a human tissue bank (Science Care, Inc., Phoenix, AZ). Arms were excluded if they were (a) from donors with a history of bone cancer or cancer that metastasizes to bone, (b) known to have been broken previously, or (c) frozen more than nine days post-mortem.

2.2. Protocol

Arms were received and kept frozen at −20 °C until the day of

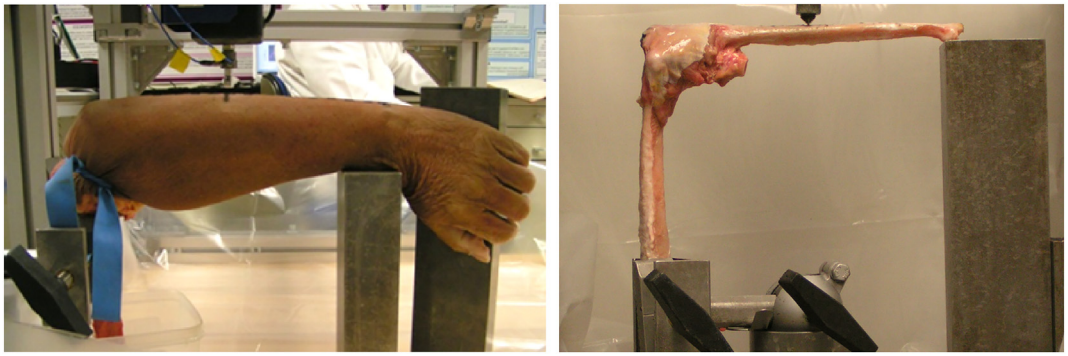

Fig. 1. Ulna support and loading in CBMT tests of the intact forearm (left) and QMT tests of excised ulnas (right).

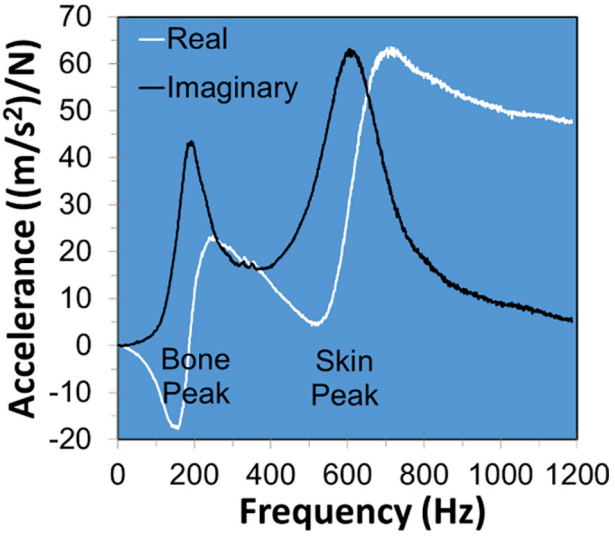

Fig. 2. Typical CBMT accelerance FRF data.

mechanical testing. Then an arm was thawed, and the upper arm was defleshed in preparation for CBMT testing of the intact forearm. Afterwards, the hand was removed, the forearm was defleshed, and the radius bone was cut at the radial tuberosity, thereby preserving the mechanical integrity of the elbow joint and preventing axial rotation of the ulna relative to the humerus. The excised ulna was then tested by QMT. After QMT testing, bones were returned to cold storage. Thus, all mechanical tests were completed in a single day. Fractured ulnas were then imaged by computed microtomography.

2.3. Data collection

2.3.1. Mechanical testing

We performed structural 3-point bending tests measuring flexural rigidity (EI) and peak moment before fracture (M_{peak}), instead of material tests reporting elastic modulus (E) and ultimate stress (σ_U), because bones fail as structures, not materials. For both CBMT and QMT data collection, the ulna was oriented horizontally with the posterior surface up (Fig. 1). The load was applied downward at the midpoint of the ulna, with the ulna supported at the elbow by the articulating vertical humerus. The humerus was secured in an adjustable bone clamp (Model #1605, Pacific Research Laboratories, Vashon, WA). For CBMT testing of the intact forearm (Fig. 1, left), the wrist was turned thumb down to position the distal ulna over the distal radius with the styloid process of the radius resting on a vertical 50 × 75 × 300 mm steel block. Axial rotation of the forearm was standardized by placing the palm against a second taller block. For QMT testing of the excised ulna (Fig. 1, right), the anterior surface of the distal radioulnar joint was supported directly on a steel block.

2.3.1.1. CBMT testing. After the forearm was mounted in the CBMT apparatus, the length of the ulna was measured with calipers and the mid-point marked on the skin. A blunt probe driven by a mechanical shaker (Model K2007E01, The Modal Shop, Inc., Cincinatti, OH) was positioned over that point. A manual linear actuator (Model VST 2015, mk Automation, Inc., Bloomfield, CT) rigidly mounted to the framework of the apparatus was used to lower the shaker-impedance head-probe assembly into contact with the forearm.

Further downward displacement of the probe applied a static load to the forearm determined by the stiffness (2.63 N/mm) of the armature suspension spring inside the shaker. Maximum displacement of the spring (9 mm) limited the applied static load to 24 N. Activation of the shaker by vibration analysis software (RT Pro, Bruel & Kjaer North America, Inc., Norcross, GA) and a dynamic signal analyzer (Photon$^+$, Bruel & Kjaer North America, Inc., Norcross, GA) superimposed a uniform (1 N) random oscillatory ($40 < f < 1200$ Hz) load on the static load. A piezoelectric impedance head (Model 288D01, PCB Piezotronics, Inc., Depew, NY) in line between the shaker and the probe was used to measure the applied oscillatory force and responding acceleration.

Fig. 2 shows the real and imaginary parts of a typical complex accelerance (acceleration divided by force) frequency response function (FRF) calculated by the vibration analysis hardware and software [44]. This FRF displays resonances at about 600 and 200 Hz. The location and shape of the higher frequency resonance is determined primarily by the mechanical properties of the skin and the applied static load, while those of the lower frequency resonance are determined primarily by the mechanical properties of the underlying bone [43]. Both resonances are also affected by damping effects of surrounding soft tissue.

2.3.1.2. Quasistatic mechanical testing. QMT data were collected under displacement control with a MTS QTest-Elite load frame (MTS Systems Corporation, Eden Prairie, MN) equipped with a 10 kN load cell (Model 4501017B, MTS Systems Corporation, Eden Prairie, MN). To prevent viscous and inertial effects from confounding elastic behavior, displacement was increased at a strain rate < 0.0001/s by setting the test frame crosshead speed to 0.1608 mm/min. Displacements of this load frame are integer multiples of 2.68 μm. By collecting data at 10 Hz at a speed of 0.1608 mm/min, one pair of displacement and force data was recorded at each 2.68 μm step (i.e., at each digital Least Significant Bit) of displacement.

Prior to loading an ulna destructively, the ulna was preconditioned by repeated loading cycles of 0–50 N, and the slopes of the load-displacement curves over the steepest 50% of the peak load were recorded. Invariably, these slopes increased monotonically from cycle to cycle toward an asymptotic limit around which they then varied randomly. Loading cycles were repeated until the coefficient of variation (CV = mean/standard deviation) in the most recent 5 cycles was < 1%.

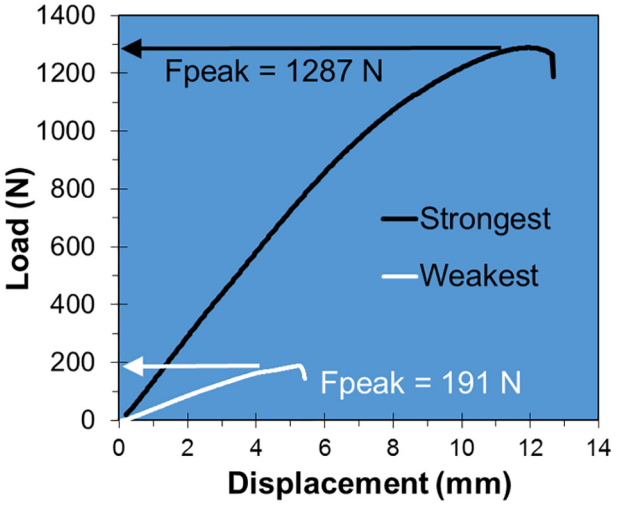

Fig. 3. QMT load/displacement curves from the weakest and strongest ulnas tested.

The number of cycles required to satisfy this criterion varied from ulna to ulna between 8 and 51. The load was then increased monotonically until the ulna fractured.

Fig. 3 illustrates the wide range of load-displacement curves observed between the weakest and strongest arms. Ulna bending strength was recorded as the peak moment prior to fracture:

$$M_{peak} = F_{peak} \times L/4 \quad (1)$$

where L was the anatomical length of the ulna measured in situ with calipers. We used the anatomical length of the ulna instead of the span between supported points within articulations, because anatomical length is what is readily measurable in vivo CBMT operators.

In quasistatic mechanical testing of bone, stiffness is usually measured as the slope of the linear portion of the load-displacement curve [45]. However, in this study of ulnas in bending, load-displacement curves displayed no extended region of linear elastic behavior (Fig. 4, left). If such behavior had existed, it would have been evident as an extended horizontal region in the associated tangent stiffness curve. Therefore, in accordance with the standard procedure for materials that do not exhibit any linear region (Paragraph A1.3 of Annex A1 in ASTM D790-3 [46], we took the maximum value of tangent stiffness as the QMT measure of ulna bending stiffness K_B. Plotting tangent stiffness as a function of load conveniently identifies both K_B and F_{peak} (Fig. 4, right).

2.3.2. Microcomputed tomography

Frozen broken ulna fragments packed in ice were shipped in thermally insulated boxes to and from the microtomographer (Microtomografix, Ltd., Sylvania, OH; microtomografix.com). As we had expected, ulnas broke under or distal to the applied load, because ulnas are narrower in the distal half. Therefore, to avoid confounding by fracture damage, ulnas were imaged slightly proximal to mid-shaft.

A μCT scanner (Model uCT 35, SCANCO Medical, Bruttisellen, Switzerland) equipped with a 2048 × 2048 CCD detector was used to make 200 cross-sectional images at 10 μm intervals along a 2 mm length of each ulna at 55% of ulna length. The scanning protocol used an X-ray tube current of 70 kVp, exposure current of 115 μA and exposure time of 750 ms. Each pixel was encoded in 16 bits for 65,536 shades of gray. Hypoxyapatite density was assumed to be 1200 mg/cm^3. Images of ulnas with diameters smaller than 20.48 mm were reconstructed over a 20.48 mm × 20.48 mm field of view and those with diameters over 20.48 mm were reconstructed over a 30.72 mm × 30.72 mm field of view for voxel sizes of 10 × 10 × 10 μm and 10 × 15 × 15 μm, respectively.

2.4. Data analysis

2.4.1. Flexural rigidity

Because slenderness ratios exceeded 12, we ignored shear effects and modeled the quasistatic behavior of the ulna as a simply supported beam in bending with stiffness K_B (Fig. 5 left). Then, to compensate for the confounding of K_B by individual differences in ulna length, we calculated ulna flexural rigidity (EI) from Euler beam theory:

$$EI = K_B \times L^3/48 \quad (2)$$

where again L was taken as the anatomical length of the ulna measured in situ with calipers.

2.4.2. CBMT data analysis

Like practitioners of MRTA [36], we modeled the forearm as a 7-parameter mechanical skin-bone system (Fig. 5, right), including the mass, stiffness and damping of the skin (M_S, K_S, D_S) and underlying bone (M_B, K_B, D_B) as well as damping by peripheral soft tissue (D_p). Solution of the differential equations of motion for this model leads to the continuous-time transfer function of the complex stiffness of the mechanical skin-bone system in the form of a 4th order rational polynomial [36]. The corresponding complex compliance of the skin-bone system is the inverse of this polynomial.

Unlike practitioners of MRTA, we estimated values of the 7 mechanical parameters by fitting the continuous-time transfer functions of both the complex stiffness and the complex compliance of the skin-bone system to the corresponding complex stiffness and compliance FRFs derived from the measured accelerance FRF of each ulna [43]. Accelerance FRFs were rejected when the root mean square of differences between paired parameter estimates from the two fits (RMS7) exceeded 9%.

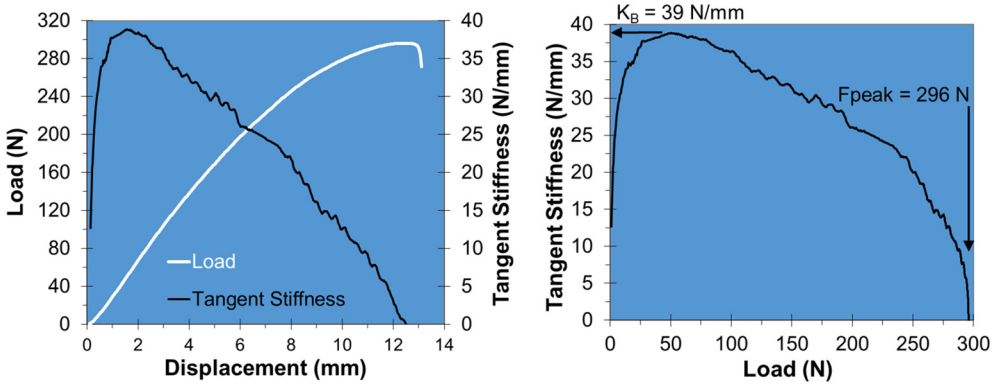

Fig. 4. Typical QMT data. Load (black) and tangent stiffness (white) as a function of displacement (left) and tangent stiffness as a function of load (right).

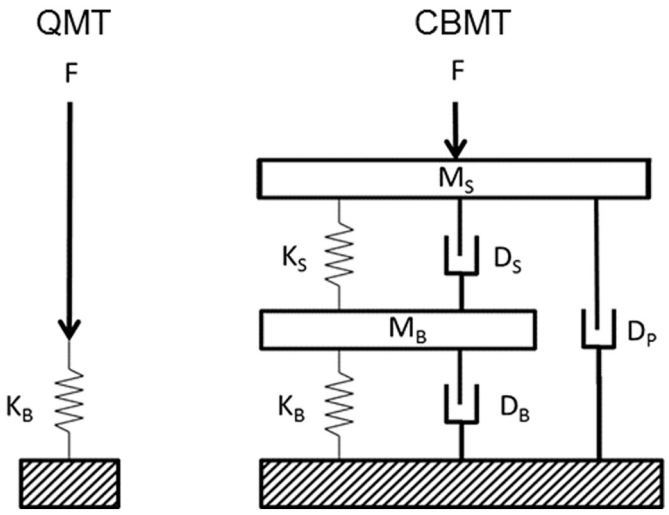

Fig. 5. Mechanical models for QMT (left) and CBMT (right) data analysis.

2.4.3. Cortical porosity

In order to provide a measure of the amount of bone loss relative to the young adult state, we defined cortical porosity to include endosteal resorption spaces. The minimum brightness in the bimodal histogram of pixel brightness was taken as the threshold distinguishing brighter bone from other darker material [59]. Endosteal and periosteal boundaries of cortical bone were outlined in slices 1, 100, and 200 along each 2 mm site. Then the BoneJ plugin [47] for the NIH image-processing software *ImageJ* [48] was used to quantify cortical porosity (CP) as the void fraction of bone volume (BV) in the total volume (TV) enclosed between the endosteal and periosteal boundaries ($CP = 1 - BV/TV$) in the entire stack of 200 images. CP was calculated three times according to the boundaries drawn in slices 1, 100, and 200. The average of the three CP values was taken as the representative measure.

In some ulnas, the endosteum was so extensively damaged by resorption that its location was ambiguous in 2D images. To resolve this ambiguity, rotatable 3D models of the entire 2 mm length at each 55% site (e.g., Fig. 6) were created with Avizo 3D visualization software (Avizo 8, FEI Visualization Sciences Group, Berlin, Germany). The endosteal *surface* revealed in these 3D models was then used to guide the drawing of the endosteal boundary in 2D images. In 5 ulnas, endosteal resorption was so extensive that the original location of the endosteum could not be seen in the 3D models. For these ulnas, endosteal area drawn as 13%, 15% and 17% of periosteal area to bracket the 15% endosteal area of the 23 year old male in Fig. 9 and a range of cortical porosities were calculated accordingly.

2.4.4. Interosseous diameter

ImageJ software was also used to measure interosseous diameter (IOD) at each 55% site as the average of the maximum periosteal diameters in slices 1, 100, and 200.

2.5. Statistical analysis

The association of CBMT and QMT measurements of ulna EI was determined by regression analysis, as were the relationships between ulna bending strength and (1) EI measured by CBMT and QMT, (2) intra-cortical porosity, (3) interosseous diameter and (4) measures of whole body size (height, weight, and BMI). Differences between means and slopes of regression lines were determined by Student's *t*-tests, and ratios of variances were determined by F-tests.

Such univariate regressions fail to quantify the extent to which predictors explain *additional* variance in a dependent variable *beyond* the amount of variance explained by other predictors. To assess the extent to which predictors explained *additional* variance, we performed a forward stepwise multiple regression in which predictors were added in order of correlation [49]. The predictors with the highest correlations with M_{peak} were EI_{QMT} ($r = 0.996$) and EI_{CBMT} ($r = 0.993$). Of these, EI_{CBMT} was chosen as the predictor in the first step, due to our interest in CBMT as a potentially clinical alternative to QMT. The predictor chosen in the second step had the highest correlation with the residuals from the regression of M_{peak} on EI_{CBMT}, and the predictor chosen in the third step had the highest correlation with residuals from the regression of EI_{CBMT} residuals on the second predictor. As will be explained in Section 3.7 below, no further steps were warranted.

Finally, to assess whether mechanical behavior differed by sex, the relationship between EI measured by CBMT and QMT was regressed separately by sex. So, too, were the regressions of M_{peak} on EI_{QMT} and on EI_{CBMT} analyzed separately by sex.

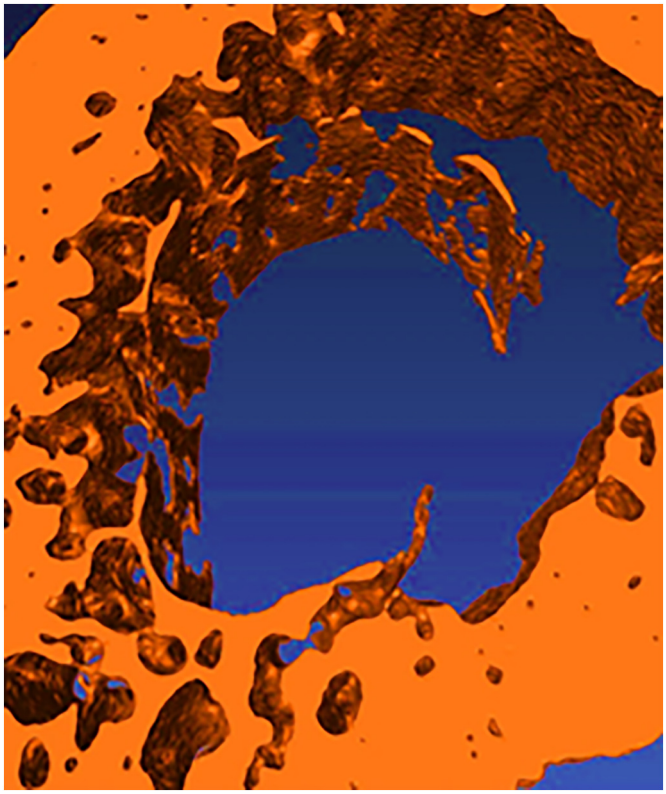

Fig. 6. 3D model of endosteal surface.

3. Results

3.1. Specimens

Arms from large men (N = 21) and small women (N = 14) ranged widely in age (17–99 years) and body mass index (13–40 kg/m^2) (Fig. 7). As expected, ulnas in these arms varied in length ($227 < L < 297$ mm), IOD at the mid-shaft ($13 < IOD < 23$ mm) and slenderness ratio ($12 < SR = IOD/L < 21$).

The ulnas also varied extensively in cross sectional form and in the patterns of cortical bone loss at the mid-shaft (Fig. 8). In this figure, the larger ulnas from large males and smaller ulnas from small females are shown at the same scale and in the same orientation of wrist rotation as in mechanical testing. The 23 year old male exemplifies undamaged cortical bone with 3% CP, and the 89 and 90 year old males illustrate the wide range of CP we found in ulnas from elderly donors (see Fig. 11 below).

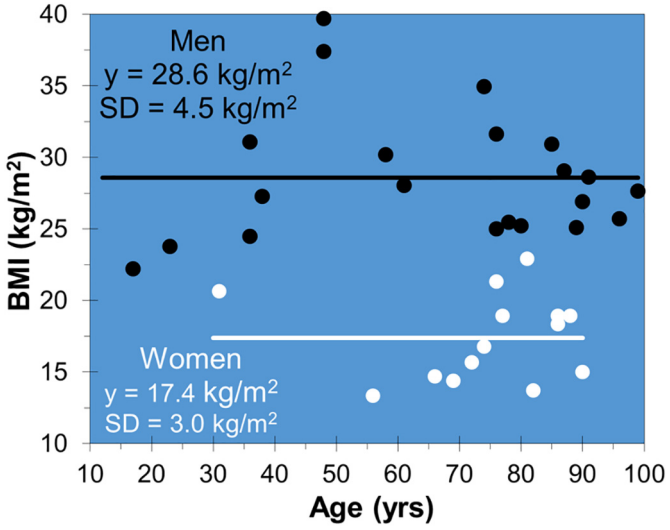

Fig. 7. Donor age and body mass index (BMI).

3.2. CBMT accuracy

As intended, QMT measurements of EI in the excised ulnas spanned a wide range (11 < EI < 69 Nm^2). CBMT measurements of EI in intact arms spanned a proportionally wider, higher range (13 < EI < 97 Nm^2). The relationship between these measurements is shown in relation to the identity line in Fig. 9, left and summarized in Table 1. The Y-intercept of the regression line was not significantly different from 0, but the slope was significantly higher than 1 (mean ± SE = 1.30 ± 0.02, $p < 0.0001$). After adjusting each CBMT measurement for this bias, the Y-intercept was still not significantly different from 0, the slope of the regression line was indistinguishable from the identity line, and the standard error of the estimate (SEE) was 3.1 Nm^2 (Table 1, Fig. 9, right). The data in Fig. 9, right were regressed separately by sex. In neither case was the Y-intercept significantly different from zero ($p \geq 0.71$), and the two slopes were indistinguishable from one another (Women: mean slope ± SE = 0.97 ± 0.03; Men: 1.01 ± 0.02, $p = 0.32$).

3.3. Prediction of ulna bending strength by EI

As intended, Mpeak varied widely (11 < M_{peak} < 90 Nm). There was no relationship between M_{peak} and age ($p = 0.67$) (Fig. 10, left). The very strong relationships between M_{peak} and ulna EI measured by QMT and by bias-adjusted CBMT are illustrated in Fig. 10, right and summarized in Table 2. Neither Y-intercept was significantly different from 0 ($p \geq 0.24$), and the slopes of the regression lines were indistinguishable ($p \geq 0.80$). For both, ulna EI explained 99% of the variance in M_{peak}, but EI_{CBMT} was less accurate than EI_{QMT} in predicting M_{peak} (SEE = 5.9 vs 4.5 Nm, F = 2.92, $p = 0.001$). Again, the data in Fig. 10, right were regressed separately by sex. In none of the four cases was a Y-intercept significantly different from zero (all $p > 0.16$), and in neither relationship did the slopes differ by sex (M_{peak} vs EI_{QMT}, Men vs Women 1.29 ± 0.02 vs 1.31 ± 0.05 Nm/Nm^2, $p = 0.72$; M_{peak} vs EI_{CBMT}, Men vs Women 1.33 ± 0.05 vs 1.27 ± 0.03 Nm/Nm^2, $p = 0.34$). Unlike other ulnas, the outlying ulna at (EI_{CBMT}, M_{peak}) = (58.1, 53.7) fractured with very little plastic deformation.

Because the slopes of the regression lines in Fig. 10, right and Fig. 9, left are strikingly similar, Mpeak was also regressed on unadjusted EI_{CBMT} values. The results in Table 2 show that the slope of this relationship was not significantly different from 1 ($p = 0.42$). That is, unadjusted measurements of EI by CBMT in intact arms (in units of Nm^2) were quantitatively indistinguishable from QMT measurements of M_{peak} in ulnas excised from those arms (in units on Nm).

3.4. Prediction of ulna bending strength by cortical porosity

As expected, CP also varied widely (3% < CP < 54%) (Fig. 11, left). Only one donor with CP > 20% was younger than 60 years of age. She was 56 years old with a BMI of 13 kg/m^2. However, CP was < 20% in 14 of the 25 donors over 60.

M_{peak} declined with CP ($p < 0.001$), but CP explained only 35% of the variance in M_{peak}. Average and ranges of CP in broad estimates of the location of the endosteum of the five ulnas in which the endosteum

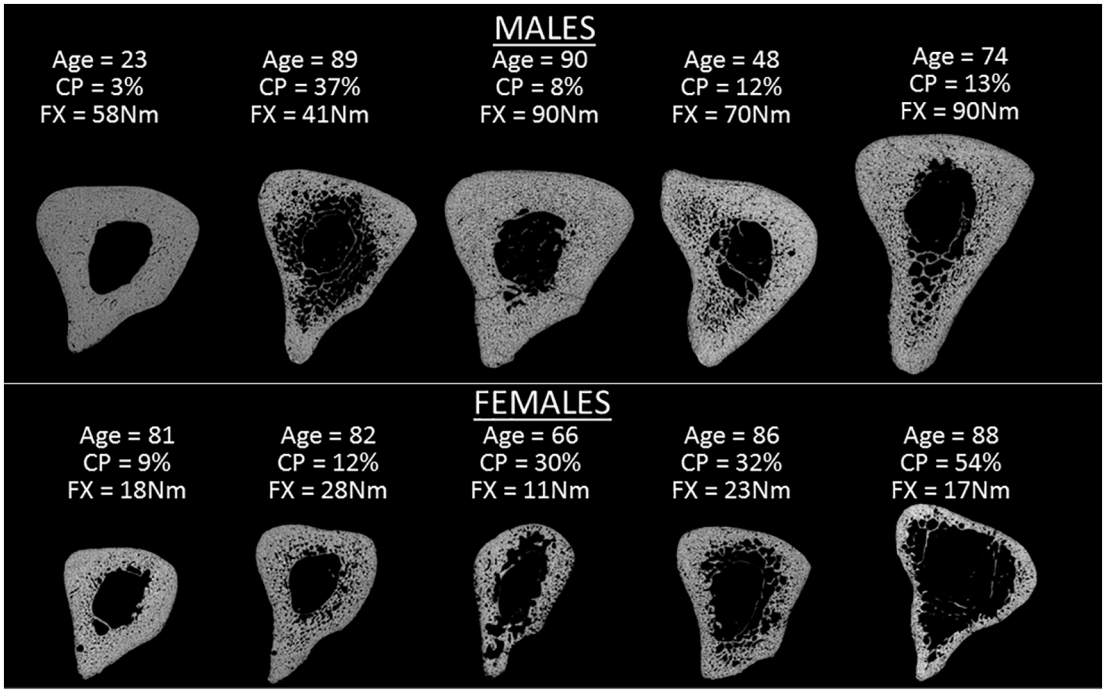

Fig. 8. Cross-sectional microtomographic images at the mid-shaft of selected ulnas.

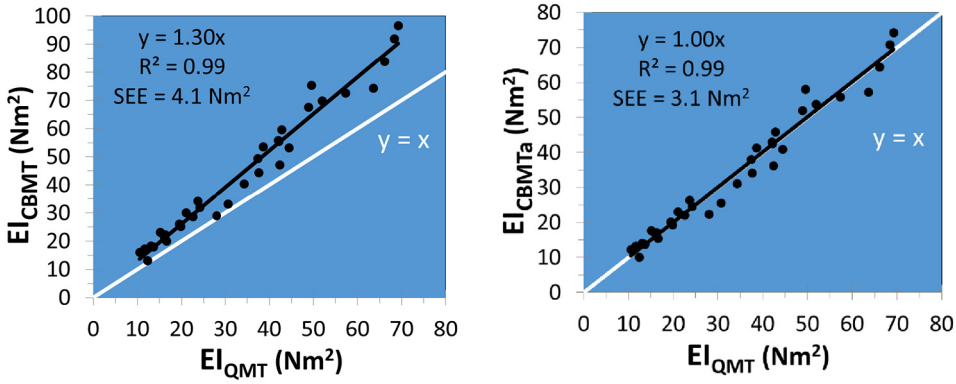

Fig. 9. Relation between EI measured by CBMT in intact arms and by QMT in excised ulnas. Left: EI_{CBMT} as measured. Right: EI_{CBMTa} = EI_{CBMT} adjusted for 1.30 bias. See Table 1.

Table 1
Regressions of ulna EI measured noninvasively by CBMT in cadaveric arms on EI measured by QMT in ulnas excised from those arms. Linear Model: $Y = b_1X + b_0$. Units: b_1 $SE(b_1)$ = dimensionless; b_0, $SE(b_0)$, SEE = Nm^2. EI_{CBMTa} = EI_{CBMT} adjusted for 1.30 bias.

Predictors	b_1	$SE(b_1)$	$p\{b_1 = 1\}$	b_0	$SE(b_0)$	$p\{b_0 = 0\}$	R^2	SEE
EI_{CBMT}	1.30	0.02	< 0.0001	0.04	1.57	0.98	0.99	4.1
EI_{CBMTa}	1.00	0.01	0.99	0.03	1.21	0.98	0.99	3.1

could not be seen in 3D models is shown in Fig. 11, right. These uncertainties had no qualitative effect on regression results. Nonlinear regression of M_{peak} on CP increased overall explained variance to 42% and reduced SEE only marginally to 17.8 Nm.

Differences in regression models (e.g., with and without a Y-intercept) require use of the standard error of the estimate (SEE) instead of R^2 for comparing prediction accuracies. By this standard, and considering both sexes together, M_{peak} was less accurately predicted by CP than by EI_{CBMT} (SEE = 18.9 vs 5.9 Nm, F = 10.45, $p < 10^{-9}$). CP was less accurate in predicting M_{peak} in ulnas with CP < 20% (SEE = 21.0 Nm) than in ulnas with CP > 20% (SEE = 14.5 Nm, F = 2.10, p = 0.02). Moreover, as shown in Table 3, the relationship between M_{peak} and CP differed between the sexes in that there was no relationship among women (p = 0.12). Accordingly, Fig. 11, right displays the mean and SD for the women.

3.5. Prediction of ulna bending strength by interosseous diameter

As expected, IOD at the mid-shaft of ulnas from large men and small women also varied widely (13 < IOD < 23 mm). The relationship between M_{peak} and IOD is shown in Fig. 12. IOD explained 79% of the variance in M_{peak}. IOD was a less accurate predictor of M_{peak} than EI_{CBMT} (SEE = 10.6 vs 5.9 Nm, F = 3.30, p < 0.001), but a more accurate predictor than CP (SEE = 18.9 vs 10.6 Nm, F = 3.17, p < 0.001).

3.6. Prediction of ulna bending strength by body size

EI_{CBMT} predicted M_{peak} more accurately than height (SEE = 14.3 Nm, F = 5.87, $p < 10^{-6}$), weight (SEE = 11.1 Nm, F = 3.54, p < 0.001) and BMI (SEE = 14.1 Nm, F = 2.39, p < 0.01). However, height (p = 0.05) weight (p = 0.001) and BMI (p = 0.05) predicted M_{peak} more accurately than CP.

3.7. Prediction of ulna bending strength by stepwise multiple regression

In the first step of the forward stepwise multiple regression, EI_{CBMT} explained R^2 = 98.6% of the variance in M_{peak} (Y = 1.28X, SEE = 5.9 Nm, F = 2398, $p = 1 \times 10^{-31}$). In the second step, the predictor most highly correlated with the residuals from the first step was age (r = −0.45). Age predicted R^2 = 20% of the variance in these residuals, corresponding to an additional 0.3% of the variance in M_{peak} (Y = −0.12X + 9, SEE = 5.3 Nm, F = 8.03, p = 0.008). No predictor less correlated than age (i.e., |r| < 0.45) explained any variance in the residuals from the first step (p > 0.2). In particular, substituting CP (r = −0.22) for age in the second step yielded R^2 = 0.05, F = 1.67 and p = 0.21. Thus, the benefit of using age as well as EI_CBMT to predict M_{peak} was to reduce SEE from 5.9 to 5.3 Nm.

In the third step, the predictor with the highest correlation with the residuals from the second step of the regression was IOD (r = −0.11). IOD explained no variance in these residuals (R^2 = 0.013, F = 0.41,

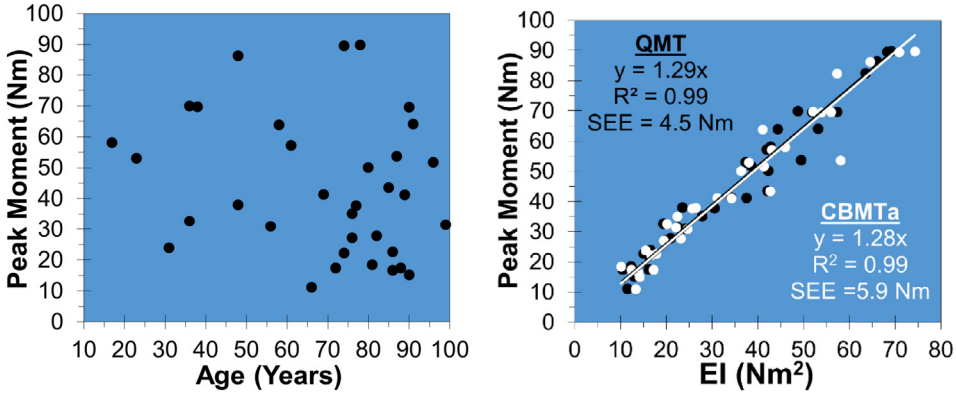

Fig. 10. Ulna bending strength (M_{peak}) measured by QMT in excised ulnas in relation to age (left) and ulna EI measured by QMT and by CBMTa in intact forearms (right). See Table 2.

Table 2
Prediction of ulna bending strength (M_{peak}) by EI_{QMT} and EI_{CBMT}. Linear Model: $Y = b_1X + b_0$. Units: b_1, $SE(b_1) = m^{-1}$; b_0, $SE(b_0)$, SEE = Nm. EI_{CBMTa} = CBMT adjusted for bias.

Predictors	b_1	$SE(b_1)$	$p\{b_1 = 1\}$	b_0	$SE(b_0)$	$p\{b_0 = 0\}$	R^2	SEE
EI_{QMT} in ulnas	1.29	0.02	< 0.001	1.5	1.7	0.37	0.99	4.5
EI_{CBMTa} in arms	1.28	0.03	< 0.001	−2.5	2.1	0.24	0.99	5.9
EI_{CBMT} in arms	0.98	0.02	0.42	2.5	2.1	0.24	0.99	5.9

p = 0.53). As in the second step, no predictor less correlated than IOD (i.e., $|r| < 0.11$) explained any variance in the residuals from the second step ($p > 0.53$). In particular, substituting CP (r = 0.004) for IOD in the third step yielded $R^2 = 1 \times 10^{-5}$, $F = 5 \times 10^{-4}$ and p = 0.98.

4. Discussion

Non-invasive measurements of ulna EI by CBMT in intact cadaveric human forearms (EI_{CBMT}) explained 99% of the variance in QMT measurements of ulna bending strength, but they were biased high by 30% relative to measurements by QMT in excised ulnas (EI_{QMT}). After adjustment for this bias, EI_{CBMTa} and EI_{QMT} fell along the identity line.

We suspect that the proportional bias in EI_{CBMT} is due to the interosseous membrane (IOM), which forms a fibrous joint, or syndesmosis, between the interosseous margins of the radius and ulna. In effect, the fibers of this membrane bind the ulna and radius into a single mechanical system [50]. They transfer longitudinal compressive loads from the distal radius to the proximal ulna and maintain transverse stability of the forearm [51]. The fibers are loose in forearm pronation and supination and taut in the neutral orientation of forearm rotation in which CBMT and QMT data are collected [51].

4.1. Prediction of ulna bending strength

Considered separately, EI was a substantially more accurate predictor of ulna bending strength than measures of ulna and whole body size, and all of these were more accurate predictors than CP. Moreover, after accounting for the influence of EI_{CBMT}, no predictor other than age explained any additional variance in ulna bending strength, and the quantitative improvement by age was only 0.3%. Indeed, considering the number, distribution and intentional confounding of age and body size in the data points of Fig. 7, the tiny influence of age detected in this study might not be reproducible in a larger, more representative sample of the population. By contrast, as the product of the ulna's elastic modulus (E) and cross-sectional moment of inertia (I), EI apparently captured the influences of all material and geometric determinants of ulna bending strength.

Table 3
Prediction of ulna bending strength (M_{peak}) by CP. Linear Model: $Y = b_1X + b_0$. Units: b_1, $SE(b_1) = m^{-1}$; b_0, $SE(b_0)$, SEE = Nm.

Group	b_1	$SE(b_1)$	$p\{b_1 = 0\}$	b_0	$SE(b_0)$	$p\{b_0 = 0\}$	R^2	SEE
All	−1.1	0.3	< 0.001	66	6	$< 10^{-11}$	0.35	18.9
Men	−0.9	0.4	0.04	69	7	$< 10^{-8}$	0.20	17.1
Women	−0.3	0.2	0.12	31	5	$< 10^{-4}$	0.19	8.2

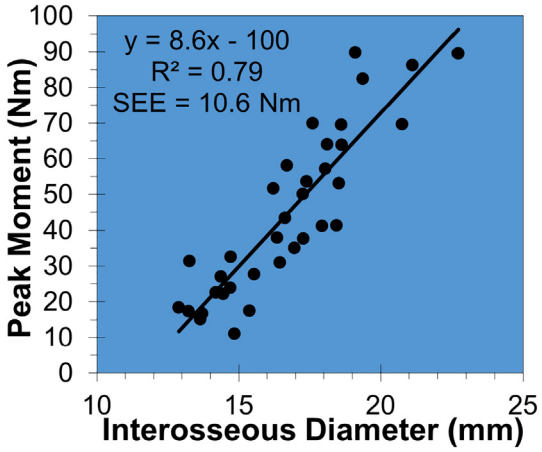

Fig. 12. The relationship between ulna bending strength (M_{peak}) and interosseous diameter (IOD).

4.2. Experimental controls

We used cadaveric human arms in this study, because the Gold Standard reference method for measuring bone stiffness and strength (QMT) can only be applied to excised bones and bone specimens. We used arms that were fresh-frozen within 9-days of refrigeration after death to ensure that in vivo bone stiffness had not yet degraded [52]. We chose arms from small women and large men to obtain a wide range of bone geometry over which to compare CBMT and QMT measurements of ulna EI, in contrast to the identical geometry of the artificial

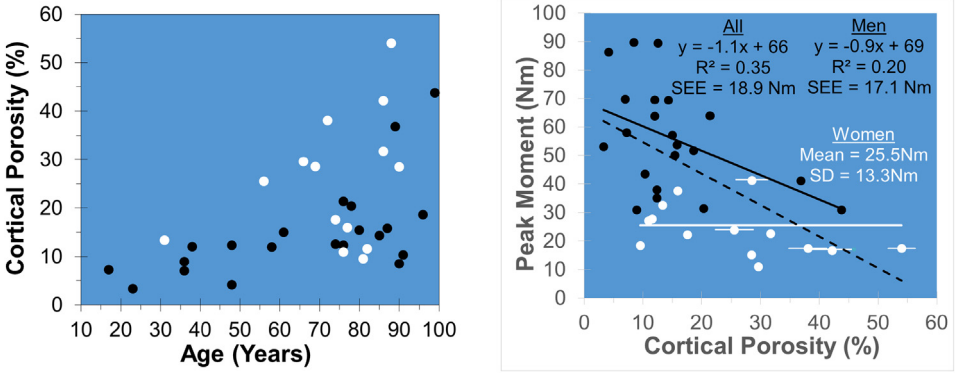

Fig. 11. Distribution of cortical porosity (CP) by age (left) and the relationship between ulna bending strength (M_{peak}) and CP (right) in ulnas from men (black) and women (white). Dashed line = All.

human ulnas that we had studied previously [43].

To fairly compare CBMT and QMT measurements of ulna EI, we closely matched end conditions in these two 3-point bending tests. We also prevented differences in axial rotation of the ulna by preserving elbow integrity, completed all tests of each arm within a single day, and kept each ulna hydrated throughout. Others using different end conditions, different axial rotations, and different values of bone length for in vivo MRTA and ex vivo QMT measurements of EI in monkey tibias in different laboratories on different days had obtained highly divergent results [29,38].

4.3. Comparisons to MRTA measurements of ulna EI

Others have reported MRTA measurements of ulna EI in vivo ranging from 16 to 41 Nm^2 in younger women [53], 12–26 Nm^2 in older women [53] and 25–78 Nm^2 in men [54]. Our own measurements of ulna EI in > 100 living human subjects have ranged from 16 Nm^2 in a small female to > 120 Nm^2 in two male weightlifters. If our speculation about the origin of the proportional bias in EI_{CBMT} is correct, then all such unadjusted noninvasive measurements of ulna EI in humans [40,53–57] should be understood as measurements of the entire radio-ulnar complex and not as measurements of the ulna alone. As Fig. 10 shows, this does not prevent ulna EI_{CBMT} from accurately predicting QMT measurements of ulna bending strength in excised ulnas.

4.4. Advantages of CBMT

As a 3-point bending test, CBMT is specifically sensitive to the mechanical properties of material at the mid-span of a long beam. As the μCT image of the ulna from the 23 year old donor in Fig. 8 illustrates, the mid-span of a long bone such as the ulna is comprised entirely of cortical bone tissue. Any apparent trabecular bone at that site (e.g., other ulnas in Fig. 8) is actually "trabecularized" residuals of cortical bone resorption. Thus, CBMT provides accurate, direct, functional measurements of the mechanical properties of unambiguously cortical bone. By contrast, analyses of cortical bone mechanics based on tomographic images of the distal forearm and lower leg suffer from uncertainty about the boundary between true trabecular and trabecularized cortical bone, as well as from the lack of patient-specific knowledge of E.

As a *dynamic* bending test, CBMT offers two important advantages over quasistatic bending tests. First, bias-adjusted CBMT accurately measures ulna EI and accurately predicts ulna bending strength in living human subjects. Second, CBMT measures the bending mass and damping of the ulna, as well as its stiffness. Few fractures occur under quasistatic conditions. Most occur under dynamic conditions in which the applied force changes rapidly with time. This rapidly changing applied force is distributed across inertial effects of bone mass and viscous effects of bone damping, as well as elastic effects of bone stiffness:

$$F(t) = M_B\, a + D_B\, v + K_B\, x \quad (3)$$

where a = acceleration, v = velocity and x = displacement of the bone. Thus, under dynamic conditions, bone mass and damping reduce the amount of force available to induce displacement, and thereby are protective against fracture. These inertial and viscous properties of bone are not susceptible to measurement by QMT.

4.5. Potential applications

Our reason for developing a CBMT test for the ulna stems from the ulna's superficiality under a thin layer of skin, and from the ulna's near ideal biomechanics in bending. By contrast, the biomechanics of the similarly superficial tibia are much more complicated, because the tibia is not rigidly supported at either the ankle or the knee. Of course, no single bone (like no single muscle) reflects the influences of other loading conditions on other bones (and muscles), but the ulna is a convenient experimental model for clinical investigations of such effects. For example, MRTA revealed a 25% increase in ulna EI after 20 weeks of resistance exercise with little or no change in BMD [40].

Beyond local loading effects, CBMT measurements of the ulna may also be useful for investigating effects of systemic influences, such as genetics, development, aging, disease, nutrition, and pharmaceuticals, on cortical bone mechanics. The mechanisms of some of these influences do not involve bone mineral. Bone mass is comprised of similar amounts of protein and mineral, and bone damping (i.e. mechanical energy dissipation) is specifically dependent on bone protein [58]. In controlled experiments, MRTA and QMT detected large protein-mediated treatment effects on EI without any change in BMD or speed of sound [42].

4.6. CBMT improvements over MRTA

Elsewhere we have described in greater detail our discovery of major sources of error in MRTA data collection and analysis, and the corrections for them that we have incorporated into CBMT [44]. One previously reported [39] source of error in MRTA data collection was failure to apply the load in the antero-posterior direction through the center of mass of the ulna, as is tacitly assumed in the mechanical model of the forearm skin-bone system (Fig. 5, right). Such misapplication of the load induces modes of vibration other than purely antero-posterior bending into the accelerance FRF data, and errors in fitting the model to the data. Indeed, it is impossible for an MRTA operator to recognize where to apply the load to avoid such errors, because soft tissue obscures imperceptible individual differences in ulna geometry and CP (Fig. 8).

A previously unreported source of error in MRTA data analysis was that estimates of model parameters obtained by fitting the 7-parameter model to FRF data are not unique. Estimates from a single FRF vary greatly with the range of frequency over which the model is fitted. Moreover, estimates obtained by fitting the model (expressed in terms of forearm stiffness) to the complex stiffness FRF differ, sometimes greatly, from estimates obtained by fitting the inverse of the model (expressed in terms of forearm compliance) to the complex compliance FRF. This conflicts with the expectation for the obverse and inverse of a function to contain the same information.

Practitioners of MRTA tried in vain to solve the data collection problem by elaborating the mechanical model to include first 9 and then 12 parameters to try to account for additional modes of vibration. Instead of changing the model, we changed the data. In CBMT, data are collected at many sites, almost all of them wrong, and the data that best conform to the 7-parameter model are identified by generally applicable, non-arbitrary, objective, quantitative criteria for preferring particular frequency ranges within particular FRFs.

Practitioners of MRTA had used the coefficient of determination (R^2) to assess the goodness-of-fit of models to data [36,40], and averaged estimates of K_B from fits with $R^2 > 0.9$ [40]. This approach led to coefficients of variation as large as 65% in repeated measures of EI made within a few minutes of one another in a single session [39]. Similarly, we found values of $R^2 > 0.98$ to be useless for preferring widely varying results of one fit over another.

We found a more discriminating statistic in the counter-intuitive discrepancies between the results of fits to the complex stiffness and compliance expressions of forearm FRF data. Finding that such discrepancies disappeared when fitting perfect synthetic 7-parameter FRF data, we recognized that these discrepancies were a measure of the non-ideality of FRF data. Indeed, values of the root mean square of paired estimates of the 7 parameters (RMS7) varied widely, with values ranging from 2% to 60%, in fits to empirical stiffness and compliance FRF data despite values of R^2 above 0.98. The CBMT results in this study used RMS7 < 9% for selecting FRFs that conform well to the 7-parameter model.

4.7. Residual variance and sources of error

Although we took care to match CBMT and QMT loading conditions, some of the disagreement between our QMT and CBMT measurements of ulna EI was surely due to several simplifications for convenience in our QMT technique for measuring ulna K_B. We treated crosshead displacement as equivalent to bending displacement. To avoid worse problems that arise with a lower range force transducer, we used a higher range force transducer to measure forces below the 20–80% range of full scale calibrated by the manufacturer. We also treated the high stiffness of the force transducer as constant over the testing range. We ignored shear, which in itself could account for errors as large as 6%. Our use of Euler beam theory to calculate ulna EI from QMT and CBMT measurements of ulna K_B, cannot be justified on theoretical grounds. Theory required us to use the span between intra-articular supports instead of the anatomical length of the ulna in the calculation, but measurement of the intra-articular span is neither convenient nor unambiguous. Beyond that, the Euler relation itself applies to prismatic beams of uniform cross section and material composition, and ulnas are far from prismatic. As others have acknowledged [36], rather than saying that an ulna *has* a particular EI, it would be more theoretically rigorous to say that the ulna *behaves* like a prismatic beam of that EI supported across a span equal to the ulna's length, but that is too verbose for colloquial use. Of course, the 7-parameter model of the forearm skin-bone system underlying the analysis of CBMT data is a simplified construct justified only by its empirical utility. Thus, despite the 99% accuracy of CBMT demonstrated in this study, known residual sources of error in the present study may present opportunities for further improvement, or more refined validation, of the technique.

4.8. Summary

CBMT offers a radiation-free means for making direct, functional measurements of the mechanical properties of unambiguously cortical bone in living human subjects. Bias-adjusted CBMT measurements of ulna EI in whole arms from donors ranging widely in age and body size were nearly identical to QMT measurements in ulnas excised from those arms. After accounting for the influence of EI_{CBMT}, no predictor other than age explained any additional variance in ulna bending strength, and the quantitative improvement by age was tiny. Thus, EI_{CBMT} effectively captures the influences of material as well as geometric factors on the mechanical properties of cortical bone. Historically, quasistatic tests have been the standard method for assessing bone mechanics, even though most fractures occur under dynamic conditions. With further research, noninvasive dynamic CBMT measurements of inertial and viscous as well as elastic properties of cortical bone may improve the targeting of fracture prevention care at individuals with weak cortical bone.

Acknowledgements

Cadaveric human arms were provided by Science Care (Phoenix, AZ). Micro-computed tomography was performed by Peter Czernik of Microtomografix, Ltd. (Sylvania, OH). Neither the sponsors nor Science Care, nor Microtomografix had any role in the study design, in the analysis and interpretation of data, in the writing of the manuscript, or in the decision to submit the manuscript for publication. The Ohio University Russ College of Technology and Engineering fabricated the force probes used for QMT and MRTA testing. Dr. Betty Sindelar of the Ohio University School of Physical Therapy made available her MTS test frame and laboratory for QMT testing. Tyler Beck, Tim Law,III, Margeaux Dennis and Maureen Dean assisted with data collection. Dr. Brian Clark of the Ohio Muscloskeletal and Neurological Institute proofed the article.

Funding

This research was funded by the Ohio Space Grant Consortium, the Ohio University Honors Tutorial College, the Ohio University Department of Biological Sciences, the Ohio University Innovation Strategy Program, and the Ohio Musculoskeletal and Neurological Institute.

Conflict of interest

ERE, GCH and JMN have nothing to disclose. LB and ABL are founders and shareholders of AEIOU Scientific, LLC.

References

[1] J. Bohannon, Osteoporosis' silent risk, Endocr. News (2013) 16–18.
[2] R. Burge, B. Dawson-Hughes, D.H. Solomon, J.B. Wong, A. King, A. Tosteson, Incidence and economic burden of osteoporosis-related fractures in the United States, 2005–2025, J. Bone Miner. Res. 22 (3) (2007) 465–475, https://doi.org/10.1359/jbmr.061113.
[3] J.A. Kanis, O. Johnell, Requirements for DXA for the management of osteoporosis in Europe, Osteoporos. Int. 16 (3) (2005) 229–238, https://doi.org/10.1007/s00198-004-1811-2.
[4] D.M. Black, C.J. Rosen, Postmenopausal osteoporosis, N. Engl. J. Med. 374 (21) (2016) 2096–2097, https://doi.org/10.1056/NEJMc1602599.
[5] J.A. Kanis, L.J. Melton 3rd, C. Christiansen, C.C. Johnston, N. Khaltaev, The diagnosis of osteoporosis, J. Bone Miner. Res. 9 (8) (1994) 1137–1141, https://doi.org/10.1002/jbmr.5650090802.
[6] S.M. Ott, When bone mass fails to predict bone failure, Calcif. Tissue Int. 53 (Suppl. 1) (1993) S7–13, https://doi.org/10.1007/BF01673395.
[7] E.S. Siris, P.D. Miller, E. Barrett-Connor, K.G. Faulkner, L.E. Wehren, T.A. Abbott, et al., Identification and fracture outcomes of undiagnosed low bone mineral density in postmenopausal women: results from the National Osteoporosis Risk Assessment, JAMA 286 (22) (2001) 2815–2822, https://doi.org/10.1001/jama.286.22.2815.
[8] K.L. Stone, D.G. Seeley, L.Y. Lui, J.A. Cauley, K. Ensrud, W.S. Browner, et al., BMD at multiple sites and risk of fracture of multiple types: long-term results from the Study of Osteoporotic Fractures, J. Bone Miner. Res. 18 (11) (2003) 1947–1954, https://doi.org/10.1359/jbmr.2003.18.11.1947.
[9] S.C. Schuit, M. van der Klift, A.E. Weel, C.E. de Laet, H. Burger, E. Seeman, et al., Fracture incidence and association with bone mineral density in elderly men and women: the Rotterdam Study, Bone 34 (1) (2004) 195–202, https://doi.org/10.1016/j.bone.2005.12.012.
[10] J.A. Pasco, E. Seeman, M.J. Henry, E.N. Merriman, G.C. Nicholson, M.A. Kotowicz, The population burden of fractures originates in women with osteopenia, not osteoporosis, Osteoporos. Int. 17 (9) (2006) 1404–1409, https://doi.org/10.1007/s00198-006-0135-9.
[11] J.A. Kanis, A. Oden, O. Johnell, H. Johansson, C. De Laet, J. Brown, et al., The use of clinical risk factors enhances the performance of BMD in the prediction of hip and osteoporotic fractures in men and women, Osteoporos. Int. 18 (8) (2007) 1033–1046, https://doi.org/10.1007/s00198-007-0343-y.
[12] J.A. Kanis, O. Johnell, A. Oden, H. Johansson, E. McCloskey, FRAX and the assessment of fracture probability in men and women from the UK, Osteoporos. Int. 19 (4) (2008) 385–397, https://doi.org/10.1007/s00198-007-0543-5.
[13] S. Boutroy, R. Zebaze, E. Sornay-Rendu, E. Seeman, R. Chapurlat, Bone microstructure identifies women without osteoporosis suffering fragility fractures: the prospective OFELY study, ASBMR Annual Meeting; October 9–12, 2015, 2015 (Seattle, WA).
[14] X. Jiang, M. Gruner, F. Tremollieres, W. Pluskiewicz, E. Sornay-Rendu, P. Adamczyk, et al., Diagnostic accuracy of FRAX in predicting the 10-year risk of osteoporotic fractures using the USA treatment thresholds: a systematic review and meta-analysis, Bone 99 (2017) 20–25, https://doi.org/10.1016/j.bone.2017.02.008.
[15] P. Augat, C.L. Gordon, T.F. Lang, H. Iida, H.K. Genant, Accuracy of cortical and trabecular bone measurements with peripheral quantitative computed tomography (pQCT), Phys. Med. Biol. 43 (10) (1998) 2873–2883, https://doi.org/10.1088/0031-9155/43/10/015.
[16] C.L. Gordon, C.E. Webber, P.S. Nicholson, Relation between image-based assessment of distal radius trabecular structure and compressive strength, Can. Assoc. Radiol. J. 49 (6) (1998) 390–397, https://doi.org/10.1118/1.597987.
[17] C. Wu, D. Hans, Y. He, B. Fan, C.F. Njeh, P. Augat, et al., Prediction of bone strength of distal forearm using radius bone mineral density and phalangeal speed of sound, Bone 26 (5) (2000) 529–533, https://doi.org/10.1016/S8756-3282(00)00250-7.
[18] C.A. Wigderowitz, C.R. Paterson, H. Dashti, D. McGurty, D.I. Rowley, Prediction of bone strength from cancellous structure of the distal radius: can we improve on DXA? Osteoporos. Int. 11 (10) (2000) 840–846, https://doi.org/10.1007/s001980070042.
[19] F. Eckstein, E.M. Lochmuller, C.A. Lill, V. Kuhn, E. Schneider, G. Delling, et al., Bone strength at clinically relevant sites displays substantial heterogeneity and is best predicted from site-specific bone densitometry, J. Bone Miner. Res. 17 (1) (2002) 162–171, https://doi.org/10.1359/jbmr.2002.17.1.162.

[20] M.E. Muller, C.E. Webber, M.L. Bouxsein, Predicting the failure load of the distal radius, Osteoporos. Int. 14 (4) (2003) 345–352, https://doi.org/10.1007/s00198-003-1380-9.
[21] R.M. Zebaze, A. Ghasem-Zadeh, A. Bohte, S. Iuliano-Burns, M. Mirams, R.I. Price, et al., Intracortical remodelling and porosity in the distal radius and post-mortem femurs of women: a cross-sectional study, Lancet 375 (9727) (2010) 1729–1736, https://doi.org/10.1016/S0140-6736(10)60320-0.
[22] G. Ioannidis, J. Flahive, L. Pickard, A. Papaioannou, R.D. Chapurlat, K.G. Saag, et al., Non-hip, non-spine fractures drive healthcare utilization following a fracture: the Global Longitudinal Study of Osteoporosis in Women (GLOW), Osteoporos. Int. 24 (1) (2013) 59–67, https://doi.org/10.1007/s00198-012-1968-z.
[23] R.L. Ohsfeldt, N.N. Borisov, R.L. Sheer, Fragility fracture-related direct medical costs in the first year following a nonvertebral fracture in a managed care setting, Osteoporos. Int. 17 (2) (2006) 252–258, https://doi.org/10.1007/s00198-005-1993-2.
[24] D.M. Cooper, C.E. Kawalilak, K. Harrison, B.D. Johnston, J.D. Johnston, Cortical bone porosity: what is it, why is it important, and how can we detect it? Curr. Osteoporos. Rep. 14 (5) (2016) 187–198, https://doi.org/10.1007/s11914-016-0319-y.
[25] R. Zebaze, E. Seeman, Cortical bone: a challenging geography, J. Bone Miner. Res. 30 (1) (2015) 24–29, https://doi.org/10.1002/jbmr.2419.
[26] L.A. Burt, J.L. Bhatla, D.A. Hanley, S.K. Boyd, Cortical porosity exhibits accelerated rate of change in peri-compared with post-menopausal women, Osteoporos. Int. 28 (4) (2017) 1423–1431, https://doi.org/10.1007/s00198-016-3900-4.
[27] D.P. Fyhrie, D. Vashishth, Bone stiffness predicts strength similarly for human vertebral cancellous bone in compression and for cortical bone in tension, Bone 26 (2) (2000) 169–173, https://doi.org/10.1016/S8756-3282(99)00246-X.
[28] S. Borders, K.R. Petersen, D. Orne, Prediction of bending strength of long bones from measurements of bending stiffness and bone mineral content, J. Biomech. Eng. 99 (1) (1977) 40–44, https://doi.org/10.1115/1.3426267.
[29] S.G. Roberts, T.M. Hutchinson, S.B. Arnaud, B.J. Kiratli, R.B. Martin, C.R. Steele, Noninvasive determination of bone mechanical properties using vibration response: a refined model and validation in vivo, J. Biomech. 29 (1) (1996) 91–98, https://doi.org/10.1016/0021-9290(95)00030-5.
[30] J.M. Jurist, A.S. Foltz, Human ulnar bending stiffness, mineral content, geometry and strength, J. Biomech. 10 (8) (1977) 455–459, https://doi.org/10.1016/0021-9290(77)90099-9.
[31] M.R. Allen, E.M. McNerny, J.M. Organ, J.M. Wallace, True gold or pyrite: a review of reference point indentation for assessing bone mechanical properties in vivo, J. Bone Miner. Res. 30 (9) (2015) 1539–1550, https://doi.org/10.1002/jbmr.2603.
[32] J.N. Farr, S. Khosla, Determinants of bone strength and quality in diabetes mellitus in humans, Bone 82 (2016) 28–34, https://doi.org/10.1016/j.bone.2015.07.027.
[33] M.A. Gallant, D.M. Brown, J.M. Organ, M.R. Allen, D.B. Burr, Reference-point indentation correlates with bone toughness assessed using whole-bone traditional mechanical testing, Bone 53 (1) (2013) 301–305, https://doi.org/10.1016/j.bone.2012.12.015.
[34] M. Granke, A. Coulmier, S. Uppuganti, J.A. Gaddy, M.D. Does, J.S. Nyman, Insights into reference point indentation involving human cortical bone: sensitivity to tissue anisotropy and mechanical behavior, J. Mech. Behav. Biomed. Mater. 37 (2014) 174–185, https://doi.org/10.1016/j.jmbbm.2014.05.016.
[35] T. Jenkins, O.L. Katsamenis, O.G. Andriotis, L.V. Coutts, B. Carter, D.G. Dunlop, et al., The inferomedial femoral neck is compromised by age but not disease: fracture toughness and the multifactorial mechanisms comprising reference point microindentation, J. Mech. Behav. Biomed. Mater. 75 (2017) 399–412, https://doi.org/10.1016/j.jmbbm.2017.06.036.
[36] C.R. Steele, L.J. Zhou, D. Guido, R. Marcus, W.L. Heinrichs, C. Cheema, Noninvasive determination of ulnar stiffness from mechanical response—in vivo comparison of stiffness and bone mineral content in humans, J. Biomech. Eng. 110 (2) (1988) 87–96, https://doi.org/10.1115/1.3108423.
[37] L.E. Miller, W.K. Ramp, C.R. Steele, S.M. Nickols-Richardson, W.G. Herbert, Rationale, design and clinical performance of the mechanical response tissue analyser: a non-invasive technology for measurement of long bone bending stiffness, J. Med. Eng. Technol. 37 (2) (2013) 144–149, https://doi.org/10.3109/03091902.2012.753128.
[38] T.M. Hutchinson, A.V. Bakulin, A.S. Rakhmanov, R.B. Martin, C.R. Steele, S.B. Arnaud, Effects of chair restraint on the strength of the tibia in rhesus monkeys, J. Med. Primatol. 30 (6) (2001) 313–321, https://doi.org/10.1034/j.1600-0684.2001.300605.x.
[39] C.E. Callaghan, Reliability of Tibial Measurement With Mechanical Response Tissue Analysis [3147769], Virginia Polytechnic Institute and State University, United States, Virginia, 2003.
[40] L.E. Miller, D.F. Wootten, S.M. Nickols-Richardson, W.K. Ramp, C.R. Steele, J.R. Cotton, et al., Isokinetic training increases ulnar bending stiffness and bone mineral in young women, Bone 41 (4) (2007) 685–689, https://doi.org/10.1016/j.bone.2007.07.004.
[41] L.E. Miller, S.M. Nickols-Richardson, D.F. Wootten, W.K. Ramp, C.R. Steele, J.R. Cotton, et al., Isokinetic resistance training increases tibial bending stiffness in young women, Calcif. Tissue Int. 84 (6) (2009) 446–452, https://doi.org/10.1007/s00223-009-9247-5.
[42] C. Wynnyckyj, S. Omelon, K. Savage, M. Damani, D. Chachra, M.D. Grynpas, A new tool to assess the mechanical properties of bone due to collagen degradation, Bone 44 (5) (2009) 840–848, https://doi.org/10.1016/j.bone.2008.12.014.
[43] P.A. Arnold, E.R. Ellerbrock, L. Bowman, A.B. Loucks, Accuracy and reproducibility of bending stiffness measurements by mechanical response tissue analysis in artificial human ulnas, J. Biomech. 47 (14) (2014) 3580–3583, https://doi.org/10.1016/j.jbiomech.2014.09.005.
[44] L. Bowman, A.B. Loucks, Improvements to Mechanical Response Tissue Analysis, MethodsX, 2019 (in press).
[45] C.H. Turner, D.B. Burr, Basic biomechanical measurements of bone: a tutorial, Bone 14 (4) (1993) 595–608, https://doi.org/10.1016/8756-3282(93)90081-K.
[46] ASTM International, D790-03 Standard Test Methods for Flexural Properties of Unreinforced and Reinforced Plastics and Electrical Insulating Materials, ASTM International, West Conshohocken, Pennsylvania, 2003, pp. 1–11.
[47] M. Doube, M.M. Klosowski, I. Arganda-Carreras, F.P. Cordelieres, R.P. Dougherty, J.S. Jackson, et al., BoneJ: free and extensible bone image analysis in ImageJ, Bone 47 (6) (2010) 1076–1079, https://doi.org/10.1016/j.bone.2010.08.023.
[48] C.A. Schneider, W.S. Rasband, K.W. Eliceiri, NIH Image to ImageJ: 25 years of image analysis, Nat. Methods 9 (7) (2012) 671–675, https://doi.org/10.1038/nmeth.2089.
[49] S. Chatterjee, B. Price, Regression Analysis by Example, John Wyley & Sons, New York, 1977 (228 pp.).
[50] D.P. Birkbeck, J.M. Failla, S.J. Hoshaw, D.P. Fyhrie, M. Schaffler, The interosseous membrane affects load distribution in the forearm, J. Hand. Surg. [Am.] 22 (6) (1997) 975–980, https://doi.org/10.1016/S0363-5023(97)80035-4.
[51] H.J. Pfaeffle, K.J. Fischer, T.T. Manson, M.M. Tomaino, S.L.-Y. Woo, J.H. Herndon, Role of the forearm interosseous ligament: is it more than just longitudinal load transfer? J. Hand. Surg. [Am.] 25A (4) (2000) 683–688, https://doi.org/10.1053/jhsu.2000.9416.
[52] R. Tennyson, R. Ewert, V. Niranjan, Dynamic viscoelastic response of bone, Exp. Mech. 12 (11) (1972) 502–507, https://doi.org/10.1007/bf02320746.
[53] F. McCabe, L.J. Zhou, C.R. Steele, R. Marcus, Noninvasive assessment of ulnar bending stiffness in women, J. Bone Miner. Res. 6 (1) (1991) 53–59, https://doi.org/10.1002/jbmr.5650060110.
[54] K.H. Myburgh, L.J. Zhou, C.R. Steele, S. Arnaud, R. Marcus, In vivo assessment of forearm bone mass and ulnar bending stiffness in healthy men, J. Bone Miner. Res. 7 (11) (1992) 1345–1350, https://doi.org/10.1002/jbmr.5650071115.
[55] G.M. Kiebzak, J.H. Box, P. Box, Decreased ulnar bending stiffness in osteoporotic Caucasian women, J. Clin. Densitom. 2 (2) (1999) 143–152, https://doi.org/10.1385/JCD:2:2:143.
[56] K.H. Myburgh, S. Charette, L. Zhou, C.R. Steele, S. Arnaud, R. Marcus, Influence of recreational activity and muscle strength on ulnar bending stiffness in men, Med. Sci. Sports Exerc. 25 (5) (1993) 592–596, https://doi.org/10.1249/00005768-199305000-00010.
[57] M.T. Liang, S.B. Arnaud, C.R. Steele, P. Hatch, A. Moreno, Ulnar and tibial bending stiffness as an index of bone strength in synchronized swimmers and gymnasts, Eur. J. Appl. Physiol. 94 (4) (2005) 400–407, https://doi.org/10.1007/s00421-005-1351-2.
[58] D.B. Burr, Why bones bend but don't break, J. Musculoskelet. Neuronal Interact. 11 (4) (2011) 270–285 (doi: http://hdl.handle.net/1805/4620).
[59] T.N. Hangartner, Thresholding technique for accurate analysis of density and geometry in QCT, pQCT and micro-CT images, J. Musculoskelet. Neuronal Interact. 7 (1) (2007) 9–16.